

# Multiple Spacecraft Assembly Maneuvers by Differential Drag and Low Thrust Engines

Riccardo Bevilacqua<sup>1</sup>, Jason S. Hall<sup>2</sup>

and

Marcello Romano<sup>3</sup>

*US Naval Postgraduate School, Monterey, California 93943*

**This work proposes a technique for optimizing the propellant consumption in multiple spacecraft assembly trajectories in Low Earth Orbits, combining the use of residual atmospheric drag and low thrust thrusters. By varying the level of aerodynamic drag of the spacecraft, relative differential accelerations are generated, and, therefore, their relative orbits are controlled. Each of the spacecraft, with the exclusion of the target, is assumed to include a system of drag plates, which can be actively opened or closed, in order to vary the atmospheric drag. Each of the spacecraft is also assumed to have continuous low thrusting capabilities in the three dimensions. In particular, the following two-phase control method is proposed. First, the relative motion of the chaser spacecraft with respect to the target spacecraft is controlled via an analytically computed differential drag sequence, with no propellant consumption, in order to move the chasers from their arbitrary initial conditions to the vicinity of the target spacecraft. Once the differential drag sequence is completed, the low thrust optimal control takes over, in order to perform an accurate rendezvous with the target spacecraft. Sample simulations are presented to support the validity and robustness of the developed technique. In particular, the Earth atmosphere is modeled to take into account day-to-night variations plus a noise effect to represent unpredictable behaviors such as “bubbles” of lower or higher density and solar effects. Furthermore, the proposed technique is validated against a complete nonlinear orbital model. The main advantage of this**

---

<sup>1</sup> Ph.D., Research Associate, Department of Mechanical and Astronautical Engineering, Code AA/RB, 699 Dyer Rd. Email: [rbevilac@nps.edu](mailto:rbevilac@nps.edu). Telephone: +1 831 656 2500. Fax: +1 831 656 2313.

<sup>2</sup> Ph.D. Candidate, Department of Mechanical and Astronautical Engineering, Code AA/JH, 699 Dyer Rd. Email: [jshall@nps.edu](mailto:jshall@nps.edu). Telephone: +1 831 656 2500. Fax: +1 831 656 2313.

<sup>3</sup> Assistant Professor, Department of Mechanical and Astronautical Engineering, Code MAE/MR, 700 Dyer Rd. Email: [mromano@nps.edu](mailto:mromano@nps.edu). Telephone: +1 831 656 2885.

**approach is that it enables a group of spacecraft to perform the assembly with very low propellant consumption.**

Keywords: Multiple Spacecraft, Differential Drag, Optimal Control, Autonomous Assembly.

### **Nomenclature**

|  |   |   |
|--|---|---|
| $a_{ISS}$  | = | ISS Orbit Semi-Major Axis   |
| $c$  | = | Coefficient in Schweighart-Sedwick Equations                                  |
| $C_D$  | = | Drag Coefficient  |
| $\Delta V$                                       | = | Fuel Consumption in terms of Total Velocity Variation                         |
| $\Delta x, \Delta y, \Delta z$                   | = | Mutual Position Coordinates of Two Spacecraft in LVLH                         |
| $\Delta \dot{x}, \Delta \dot{y}, \Delta \dot{z}$ | = | Mutual Velocity Components of Two Spacecraft in LVLH                          |
| $\Delta S$                                       | = | Difference in cross wind section area between two spacecraft                  |
| $\Delta t^*$                                     | = | Unknown Time Duration for the Controlled Rendezvous Phases                    |
| $\Delta t_w$                                     | = | Waiting Time Interval before Controlled Phase in Rendezvous Maneuver          |
| $e$  | = | Time-Varying Eccentricity of the Harmonic Oscillator Motion                   |
| $e_0$  | = | Time-Varying Eccentricity of the Harmonic Oscillator Motion before Rendezvous |
| $e_{ISS}$  | = | ISS Orbit Eccentricity  |
| $\Phi(t)$  | = | state transition matrix for Clohessy-Wiltshire, 1960 equations                |
| $\phi$   | = | Phase of Forcing Term in Out-of-plane Motion in Schweighart-Sedwick Equations |
| $h$  | = | Target Altitude above the Earth Surface                                       |
| $I$  | = | Fuel Consumption in terms of Total Impulse                                    |
| $\mathbf{I}$                                     | = | Identity Matrix   |
| ISS  | = | International Space Station   |
| $i_{ref}$  | = | Reference LVLH Orbit Inclination  |
| $i_{ISS}$  | = | ISS Orbit Inclination   |

|                   |   |  |
|-------------------|---|--|
| $J_2$             | = | Second Order Harmonic of Earth Gravitational Potential Field (Earth Flattening) [ $108263 \times 10^{-8}$ , Vallado] |
| $J$               | = | cost function  |
| LVLH              | = | Local Vertical Local Horizontal  |
| $l$               | = | Coefficient in Schweighart-Sedwick Equations (out-of-plane motion)   |
| $\bar{\lambda}_r$ | = | position adjoint vector  |
| $\bar{\lambda}_v$ | = | velocity adjoint vector  |
| $m$               | = | Spacecraft Mass  |
| $v_{ISS}$         | = | ISS Orbit Initial Anomaly  |
| $\omega$          | = | Orbital Angular rate of the Target   |
| $\omega_{ISS}$    | = | ISS Orbit Argument of Perigee  |
| $\Omega$          | = | ISS Orbit Right Ascension of Ascending Node (RAAN)   |
| $\Psi(t)$         | = | convolution integral matrix for Clohessy-Wiltshire, 1960 equations due to optimal unbounded control                  |
| $q$               | = | Coefficient in Schweighart-Sedwick Equations (out-of-plane motion)   |
| $\vec{r}$         | = | relative position vector   |
| $R_{\oplus}$      | = | Earth Mean Radius [ $6378.1363 \text{ km}$ , Vallado]  |
| $r_{ref}$         | = | Reference LVLH Orbit Radius  |
| $\rho$            | = | Atmospheric Density  |
| $S$               | = | Spacecraft Wind-Cross Section Area   |
| $S_p$             | = | Single Plate Wind-Cross Section Area   |
| $T$               | = | Orbital Period   |
| $t$               | = | Time   |
| $u, U$            | = | Control Variable   |
| $V$               | = | Spacecraft Velocity Vector Magnitude with respect to Earth Atmosphere  |
| $\hat{V}$         | = | Spacecraft Velocity Unit Vector with respect to Earth Atmosphere   |

$\vec{v}$  = relative velocity vector in LVLH

$\mathbf{z}' = [z'_1 \ z'_2 \ z'_3 \ z'_4]^T$  = Intermediate Transformed Spacecraft Relative State Vector

$\mathbf{z} = [z_1 \ z_2 \ z_3 \ z_4]^T$  = Transformed Spacecraft Relative State Vector

$(\dots)_0$  = Initial Conditions

$(\dots)_j$  = Component along  $j$  direction in LVLH ( $j = x, y, z$ )

## I. Introduction

This work proposes the integration of differential drag-based control and low-thrust optimal control for multiple spacecraft rendezvous and assembly maneuvers.

The possibility of controlling spacecraft relative motion by exploiting the Earth's atmosphere, combined with ad-hoc-driven vehicles' relative configuration, has been studied for several years (Leonard 1986, Leonard et al. 1989, Humi et al., 2001 and 2003, Carter et al., 2002, Palmerini et al., 2005) and it is still an open topic of research (Shankar et al., 2008, Bevilacqua et al., 2008). When atmospheric differential drag is used for satellites rendezvous, an under-actuated controllable system is introduced, as already discussed in previous literature (Campbell et al., 2003, Kumar et al., 2007 and Starin et al., 2001).

Spacecraft rendezvous and assembly has also been addressed in order to optimize propellant consumption, by allowing long time duration low-thrust maneuvers (Bevilacqua et al. 2007, Guelman et al., 2001 and Humi et al., 2001).

In this work we propose a new approach based on the combination of differential drag and low-continuous-thrust optimal control, in order to generate quasi propellant-free assembly maneuvers for an arbitrary number of spacecraft. The approach of the chaser spacecraft to a target spacecraft is performed via differential drag from far away initial conditions, until the vicinities are reached. Then, low-thrust engines are used to complete the precise rendezvous. Both controllers, which are based on linear dynamics and simplifying assumptions are validated against an high fidelity orbital propagator, in order to evaluate their robustness and feasibility. In particular, part of the differential drag controller and the whole optimal thrust controller are implemented as feedback reactions with respect to the spacecraft relative states.

The main contributions of this paper to the state of the art for multiple spacecraft assembly control can be summarized as follows:

1. Introduction of a new hybrid technique to obtain low propellant spacecraft rendezvous and assembly maneuvers.
2. Further development of previously obtained analytical results on differential drag precise rendezvous (Bevilacqua and Romano, 2008).
3. Demonstration of a seamless integration between existing rendezvous optimal controller (Guelman et al., 2001) and differential drag controller.
4. Test of linear models based techniques against a complete nonlinear model which includes disturbances and uncertainties on the atmospheric density.

The paper is organized as follows. Section II introduces the dynamics model and control logic used for the differential drag controller design. Section III illustrates the optimal low-thrust approach for the final phase of the assembly maneuver. Section IV describes the validation of the drag controller and the optimal low-thrust controller with a nonlinear orbital propagator and a realistic spacecraft model. Section V is dedicated to numerical simulations and section VI concludes the paper.

## II. Dynamics Model including $J_2$ and Control via Differential Drag

In this section the analytical developments for the dynamics and control of the spacecraft relative motion via differential drag are presented. The differential drag control logic is used in the first phase of the multi-spacecraft assembly maneuvers.

The relative dynamics between two generic spacecraft, considering the averaged effect of the  $J_2$  perturbation over one orbit, projected in the LVLH coordinate system, is represented by the Schweighart-Sedwick equations (Schweighart-Sedwick, 2002)

$$\begin{cases} \Delta\ddot{x} = 2(\omega c)\Delta\dot{y} + (5c^2 - 2)\omega^2\Delta x + u_x \\ \Delta\dot{y} = -2(\omega c)\Delta\dot{x} + u_y \\ \Delta\ddot{z} = -q^2\Delta z + 2lq\cos(qt + \phi) + u_z \end{cases} \quad (1)$$

The Schweighart-Sedwick LVLH coordinate system is defined as follows: the  $x$  axis points from the center of the Earth to the origin of the system (which moves along a circular orbit), the  $y$  axis is along the orbital track and

the  $z$  axis completes a right-hand Cartesian coordinate system. The angular velocity of the coordinate system with respect to an inertial frame is defined as  $\omega c$ , being  $c$  defined in Eq. (2)

$$c = \sqrt{1 + \frac{3J_z R_{\oplus}^2}{8r_{ref}^2} (1 + 3\cos 2i_{ref})} \quad (2)$$

Furthermore,  $[u_x \ u_y \ u_z]$  indicate the components of the relative acceleration between the two spacecraft.

When only differential drag is considered, the control vector becomes

$$[u_x \ u_y \ u_z] = \left[ 0 \ \left( -\frac{\rho \Delta S C_D V^2}{2m} \right) \ 0 \right] \quad (3)$$

The dynamics of Eq. (1) can be decomposed into a double integrator and a harmonic oscillator via the following state vector transformation

$$\begin{bmatrix} z'_1 \\ z'_2 \\ z'_3 \\ z'_4 \end{bmatrix} = \begin{bmatrix} 0 & 1 & -\frac{A}{A^2 - B} & 0 \\ -\frac{BA}{A^2 - B} & 0 & 0 & -\frac{B}{A^2 - B} \\ 0 & 0 & -\frac{A^2}{2(A^2 - B)^{3/2}} & 0 \\ -\frac{A^2 B}{2(A^2 - B)^{3/2}} & 0 & 0 & -\frac{A^3}{2(A^2 - B)^{3/2}} \end{bmatrix} \begin{bmatrix} \Delta x \\ \Delta y \\ \Delta \dot{x} \\ \Delta \dot{y} \end{bmatrix}; \quad A = 2(\omega c), B = (5c^2 - 2)\omega^2 \quad (4)$$

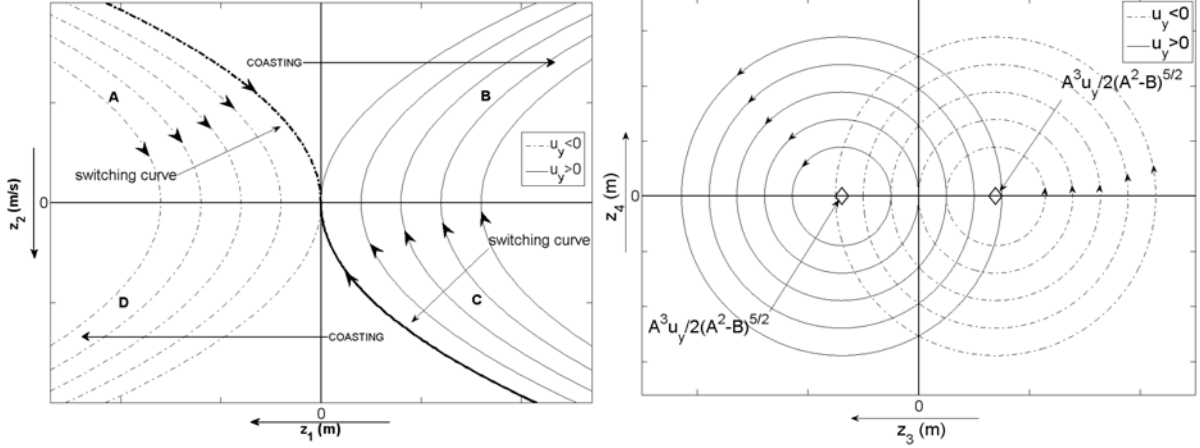
The dynamics in the new state vector (see also Bevilacqua and Romano, 2008) has the following closed form solution for constant control acceleration  $u_y$  with  $u_x = u_z = 0$

$$\begin{aligned} z'_1 &= -\frac{B}{A^2 - B} u_y \frac{t^2}{2} + z'_{2_0} t + z'_{1_0} \\ z'_2 &= -\frac{B}{A^2 - B} u_y t + z'_{2_0} \\ z'_3 &= \left( z'_{3_0} - \frac{A^3 u_y}{2(A^2 - B)^{5/2}} \right) \cos \left[ \left( \sqrt{A^2 - B} \right) t \right] + \frac{z'_{4_0}}{\sqrt{A^2 - B}} \sin \left[ \left( \sqrt{A^2 - B} \right) t \right] + \frac{A^3 u_y}{2(A^2 - B)^{5/2}} \\ z'_4 &= z'_{4_0} \cos \left[ \left( \sqrt{A^2 - B} \right) t \right] - \sqrt{A^2 - B} \left( z'_{3_0} - \frac{A^3 u_y}{2(A^2 - B)^{5/2}} \right) \sin \left[ \left( \sqrt{A^2 - B} \right) t \right] \end{aligned} \quad (5)$$

For notation convenience we use, for the rest of the paper, the following modified final transformed state vector

$$\begin{aligned}
z_1 &= z'_1 \\
z_2 &= z'_2 \\
z_3 &= z'_3 \\
z_4 &= \frac{z'_4}{\sqrt{A^2 - B}}
\end{aligned} \tag{6}$$

The two aspects of the relative motion dynamics can be represented in two different phase planes. Figure 1 a represents the double integrator motion, Figure 1 b the harmonic oscillator part.



a) Qualitative shape of the curves in  $z_1 z_2$

b) Qualitative shape of the curves in  $z_3 z_4$

**Figure 1 Qualitative shape of the curves representing the relative motion of a chaser with respect to the target in the phase planes. The axis orientation has been chosen consistently with Leonard 1986, 1989.**

When using differential drag as control, drag plates are imagined to be mounted on each spacecraft, so that the relative acceleration sign can be controlled (see Eq. (3):  $\Delta S$  can be either zero, negative or positive). Furthermore, the following assumptions are made, in order to exploit the analytical solution in Eq. (5) for designing the control logic (Bevilacqua, 2008). It is important to highlight that the assumptions listed below are only used for the analytical developments of the drag control logic.

1. The angle of attack of the drag plates of each spacecraft can be either 0 or 90 degrees, thus generating a minimum (Figure 2, CASE 1), zero (Figure 2, CASE 2) or a maximum (Figure 2, CASE 3) relative drag acceleration. Furthermore, the drag plates are considered to rotate in couples, as depicted in Figure 2, CASE 2.
2. Attitude dynamics is not considered. Attitude is assumed to be stabilized in the LVLH coordinate system.

3. All of the spacecraft in the fleet have the same drag coefficient and mass.
4. The air density is constant for all of the spacecraft and equal to that of the target's altitude at the initial time  $t_0$ .
5. The problem is confined to the  $xy$  plane. Therefore, for each chaser, the state vector is  $[\Delta x \ \Delta y \ \Delta \dot{x} \ \Delta \dot{y}]^T$  and the final condition is  $[\Delta x \ \Delta y \ \Delta \dot{x} \ \Delta \dot{y}]^T = [0 \ 0 \ 0 \ 0]^T$ . The dynamics along the  $z$  axis, which is oscillatory and independent from the one on the  $xy$  plane, is controlled only in the last phase of the maneuver, when thrusters take over.
6. The target orbital rate  $\omega$  is constant during the maneuver.

Assumptions 4 and 6 are removed when the complete nonlinear model is used to test the controller in the simulations section (Section V).

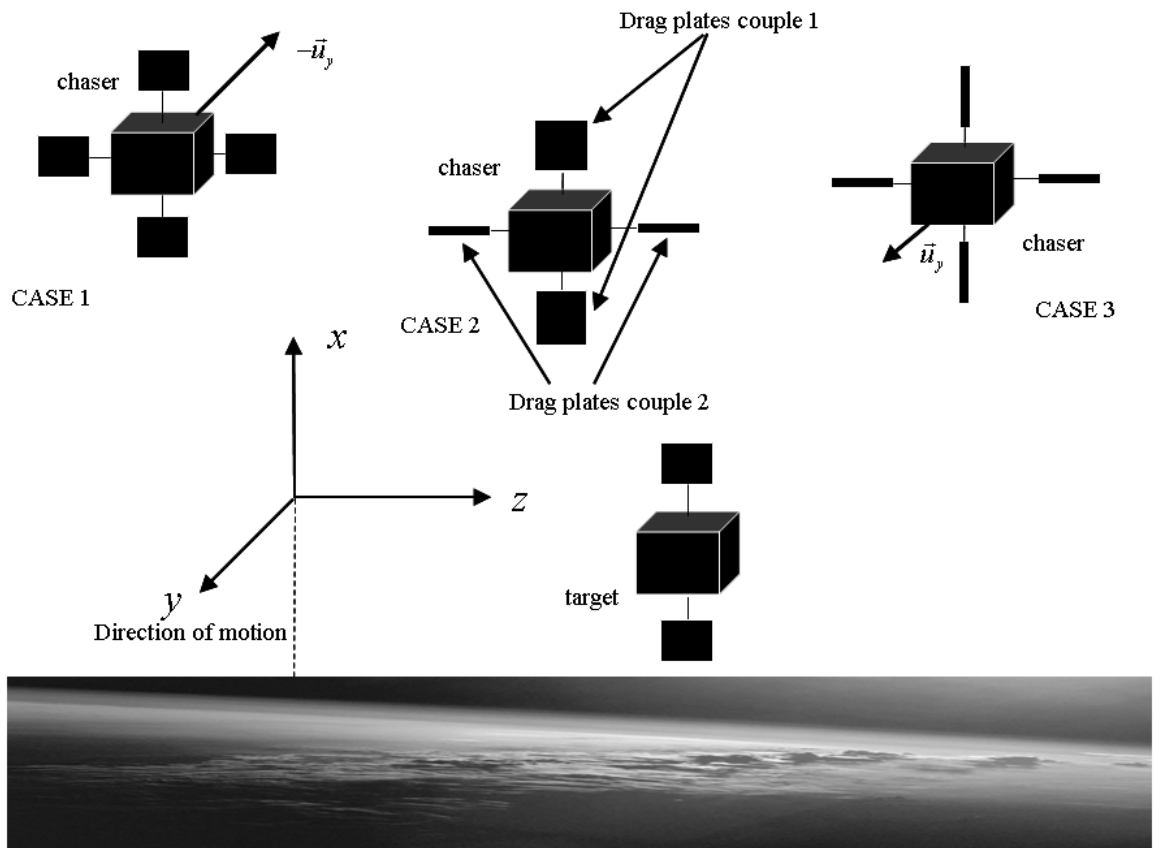


**Figure 2 Drag Plates Concept.**

The drag plates concept illustrated in Figure 2 represents an evolution of the idea previously introduced by Bevilacqua and Romano, 2008. In particular, in this paper the target spacecraft is not controlling its surfaces'

orientation, while each individual chaser is capable of generating a negative, zero or positive control with respect to the target. By this new assumption we simplify the algorithm presented in Bevilacqua and Romano, 2008, by removing any mutual constraints among the control signs of the chasers.

The control sequence is divided in two phases:

1. Stabilization of the chasers with respect to the target, i.e. canceling out the double integrator motion so that the chasers orbit around the target in a stable motion (see Figure 3). The stable motion can be either a leader-follower configuration or a closed relative orbit described by the chaser around the target.
2. After stabilization, precise rendezvous at the target is obtained by an analytically determined control sequence (see Figure 4)

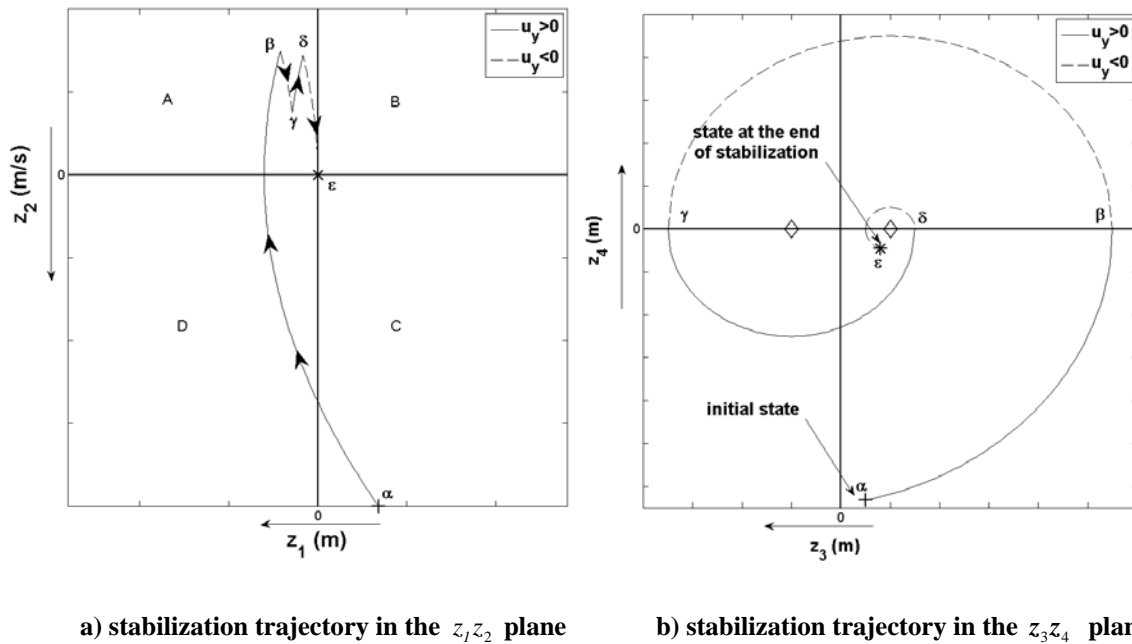


**Figure 3** Qualitative example of relative orbit stabilization maneuver in the phase planes. The plus symbol (+) on the trajectory indicates the initial state, the star symbol (\*) indicates the final condition at the exit of the stabilization algorithm. Equal Greek letters in the two figures indicate simultaneous events.

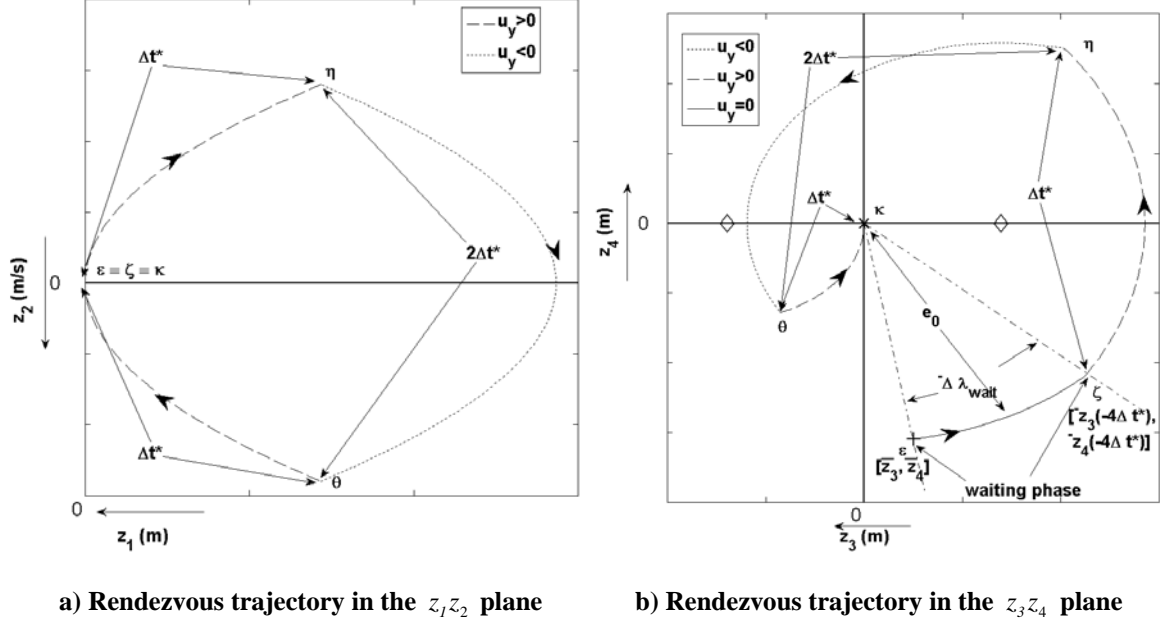


**Figure 4** Qualitative example of rendezvous maneuver in the phase planes. In figure b the plus symbol (+) indicates the initial state, and the star symbol (\*) indicates the final condition.

In particular the value of  $\Delta t^*$  used in the control sequence in Figure 4 is (Bevilacqua and Romano, 2008)

$$\Delta t^* = \frac{1}{f} \cos^{-1} \left( \frac{\left( \frac{1}{2} + \left( \frac{1}{12} \right) \sqrt{36 + \frac{6\sqrt[3]{H}}{K} - \frac{36e_0^2}{K\sqrt[3]{H}}} \right) \left( \frac{\sqrt{6}}{12} \right) \sqrt{12 - \frac{\sqrt[3]{H}}{K} + \frac{6e_0^2}{K\sqrt[3]{H}}} - \frac{72}{\sqrt{36 + \frac{6\sqrt[3]{H}}{K} - \frac{36e_0^2}{K\sqrt[3]{H}}}} \right)}{\left( \frac{1}{2} + \left( \frac{1}{12} \right) \sqrt{36 + \frac{6\sqrt[3]{H}}{K} - \frac{36e_0^2}{K\sqrt[3]{H}}} \right) \left( \frac{\sqrt{6}}{12} \right) \sqrt{12 - \frac{\sqrt[3]{H}}{K} + \frac{6e_0^2}{K\sqrt[3]{H}}} - \frac{72}{\sqrt{36 + \frac{6\sqrt[3]{H}}{K} - \frac{36e_0^2}{K\sqrt[3]{H}}}} \right)} \right) \quad (7)$$

$$H = -54Ke_0^2 + 6\sqrt{3}e_0^2\sqrt{2e_0^2 + 27K^2},$$

$$f = \sqrt{A^2 - B}, \quad K = -\frac{\sqrt{2}}{2} \frac{A^3 |u_y|}{f^5} i$$

The following statement constitutes an important new development with respect to Bevilacqua and Romano, 2008. In order for the argument of the inverse cosine in Eq. (7) not to exceed the unit value the following condition needs to hold true

$$e_0 = \sqrt{z_3^2 + z_4^2} < \frac{13}{5} \frac{A^3 u_y}{(A^2 - B)^{5/2}} \quad (8)$$

If this condition is not satisfied at the beginning of the rendezvous phase, the sequence of Figure 4 must be repeated until the quantity  $\sqrt{z_3^2 + z_4^2}$  respects the constraint of Eq. (8). In other words, the rendezvous sequence is

performed by reducing the amplitude of the harmonic motion  $\sqrt{z_3^2 + z_4^2}$  from the initial value  $e_0$ , after the stabilization phase, to intermediate values  $e_1, e_2, \dots, e_N$ , until the sequence can drive it to zero, once the condition in Eq. (8) is satisfied at the  $e_N$ .

Considering a generic iteration of the algorithm between the state vector magnitudes  $e_j$  and  $e_{j+1}$ , with  $(e_j - e_{j+1}) = \frac{13}{5} \frac{A^3 u_y}{(A^2 - B)^{5/2}} - \varepsilon$ , where  $\varepsilon$  is a user selectable small quantity, Eq. (7) is substituted by

$$\Delta t^* = \frac{1}{f} \cos^{-1} \left( \frac{\frac{1}{2} + \left(\frac{1}{12}\right) \sqrt{36 + 6\sqrt[3]{H}/K - 36(e_j - e_{j+1})^2 / K^3 \sqrt[3]{H}}}{\left(\frac{\sqrt{6}}{12}\right) \sqrt{12 - \sqrt[3]{H}/K + 6(e_j - e_{j+1})^2 / K^3 \sqrt[3]{H}} - \frac{72}{\sqrt{36 + 6\sqrt[3]{H}/K - 36(e_j - e_{j+1})^2 / K^3 \sqrt[3]{H}}}} \right) \quad (9)$$

$$H = -54K(e_j - e_{j+1})^2 + 6\sqrt{3}(e_j - e_{j+1})^2 \sqrt{2(e_0 - e_1)^2 + 27K^2}$$

Collision avoidance issues are solved by recomputing the chasers' trajectories, iterating on the value of the initial coasting phase, as described in Bevilacqua and Romano, 2008. Since the drag control sequence is completely analytical, these iterations can be performed with very low computational burden.

### III. Optimal Low-Thrust Close Proximity Maneuvers

Using the linear model based control sequence described in previous section against a true orbital nonlinear model introduces errors in matching the final desired state vector for the chaser spacecraft. Furthermore, the differential drag control presented does not deal with the out of plane motion. For these reasons, an optimal controller, based on low thrust engines, is proposed for the last phase. This section builds upon the results of Guelman et al., 2001.

The Clohessy-Wiltshire equations are used here to represent the relative state vector evolution between two generic spacecraft (Eq. 10). The use of this simpler representation of the relative motion with respect to Eq. (1) enables to usefully exploit the optimality conditions and it will be validated by the numerical simulations of Section V. In particular, if the chasers are already in the vicinities of the target, the simple HCW model can be used with no major issues due to the linear approximation and neglecting of disturbances. Furthermore, in order to overcome this

limitation, and to be able to use the fuel optimal HCW-based approach for distances of the order of several kilometers, the solution of Guelman et al, 2001 is implemented in such a way that it can be repetitively computed at fixed time steps, in a feedback fashion with respect to the spacecraft relative state vector, so that nonlinear effects and disturbances can be satisfactorily dealt with.

The Hill-Clohessy-Wiltshire equations can be written as

$$\begin{bmatrix} \Delta\dot{x} \\ \Delta\dot{y} \\ \Delta\dot{z} \\ \Delta\ddot{x} \\ \Delta\ddot{y} \\ \Delta\ddot{z} \end{bmatrix} = \begin{bmatrix} 0 & 0 & 0 & 1 & 0 & 0 \\ 0 & 0 & 0 & 0 & 1 & 0 \\ 0 & 0 & 0 & 0 & 0 & 1 \\ 0 & 0 & 0 & 0 & 2\omega & 0 \\ 0 & 3\omega^2 & 0 & -2\omega & 0 & 0 \\ 0 & 0 & -\omega^2 & 0 & 0 & 0 \end{bmatrix} \begin{bmatrix} \Delta x \\ \Delta y \\ \Delta z \\ \Delta\dot{x} \\ \Delta\dot{y} \\ \Delta\dot{z} \end{bmatrix} + \begin{bmatrix} 0 \\ 0 \\ 0 \\ u_x \\ u_y \\ u_z \end{bmatrix} \quad (10)$$

with the LVLH angular velocity given by  $\omega = 2\pi/T$ . By defining

$$\vec{r} = \begin{bmatrix} \Delta x \\ \Delta y \\ \Delta z \end{bmatrix}, \quad \vec{V} = \begin{bmatrix} \Delta\dot{x} \\ \Delta\dot{y} \\ \Delta\dot{z} \end{bmatrix}, \quad \vec{u} = \begin{bmatrix} u_x \\ u_y \\ u_z \end{bmatrix}, \quad A_1 = \begin{bmatrix} 0 & 0 & 0 \\ 0 & 3\omega^2 & 0 \\ 0 & 0 & -\omega^2 \end{bmatrix}, \quad A_2 = \begin{bmatrix} 0 & 2\omega & 0 \\ -2\omega & 0 & 0 \\ 0 & 0 & 0 \end{bmatrix} \quad (11)$$

and assuming continuous thrust capability in three dimensions, the propellant optimal control problem can be stated as follows (Guelman et al, 2001). Given the initial and final conditions for the state vector  $[\vec{r}^T \quad \vec{V}^T]^T$  and a time interval to perform the maneuver  $\Delta t = t_2 - t_1$ , minimize the cost function

$$J = \frac{1}{2} \int_{t_1}^{t_2} (\vec{u})^T \cdot (\vec{u}) dt \quad (12)$$

subject to the constraints

$$|u_k| \leq u_{\max}, \quad k = x, y, z \quad (13)$$

In our particular case, the initial state vector of the generic chaser spacecraft is taken to be the state at the end of the differential drag control phase and the final desired state vector is the 6-by-1 null vector.

The Hamiltonian of the problem is

$$H = \frac{1}{2} \vec{u} \cdot \vec{u} + \vec{\lambda}_r^T \cdot \vec{V} + \vec{\lambda}_v^T \cdot (A_1 \vec{r} + A_2 \vec{V} + \vec{u}) \quad (14)$$

By applying the minimum principle (Pontryagin et al., 1969) and considering the constraints in Eq. (13), the optimal control law is given by

$$\begin{aligned}
 u_k &= -\lambda_{v_k} & \text{if} & \quad \left| \lambda_{v_k} \right| \leq u_{\max}, \quad k = x, y, z \\
 u_k &= -\text{sign}(\lambda_{v_k}) u_{\max} & \text{if} & \quad \left| \lambda_{v_k} \right| > u_{\max}, \quad k = x, y, z
 \end{aligned} \tag{15}$$

Moreover, the time evolution of the costate needed in Eq. (15) is described by

$$\begin{Bmatrix} \dot{\bar{\lambda}}_r \\ \dot{\bar{\lambda}}_v \end{Bmatrix} = - \begin{bmatrix} 0 & \mathbf{I} \\ \mathbf{A}_1 & \mathbf{A}_2 \end{bmatrix}^T \begin{Bmatrix} \bar{\lambda}_r \\ \bar{\lambda}_v \end{Bmatrix} \tag{16}$$

We consider each thrust component to be generated by an independent continuously operated actuator. The optimal control problem is solved by iteratively searching for the values of the initial condition of the costate vector that minimizes the norm of the error between the desired and actual final states. This error is found by propagating Eq. (10), with the control policy of Eq. (15). The initial time costate vector guess for the first iteration is chosen as the one for the unconstrained continuous control

$$\bar{\lambda}_0 = -\Psi^{-1}(t_f - t_0) \left[ \Phi(t_f - t_0) \begin{bmatrix} \bar{\mathbf{r}}_0 \\ \bar{\mathbf{v}}_0 \end{bmatrix} - \begin{bmatrix} \bar{\mathbf{r}}_f \\ \bar{\mathbf{v}}_f \end{bmatrix} \right] \tag{17}$$

being  $\Psi(t)$  the convolution integral for the state vector due to the optimal unbounded control and  $\Phi(t)$  the state transition matrix associated to the dynamics in Eq. (10) (see Guelman et al., 2001 for details).

The Matlab® *fminsearch* routine is used to efficiently solve the numerical problem.

#### IV. Implementation of the Differential Drag and Optimal Low-Thrust Controllers

Having laid out the mathematical background to both the proposed differential drag-based and optimal low-thrust controllers, this section is detailing the practical implementation of the algorithms. The block diagram of an integrated spacecraft control system with the differential drag controller and optimal low-thrust controller is presented in Figure 5. The inputs to the differential drag controller are the current position and velocity of the spacecraft in the Schweighart-Sedwick LVLH frame and its velocity in the inertial frame. Additionally, the spacecraft's surface area, its coefficient of drag, the drag plates surface areas, the atmospheric density at the target's

altitude at start time, and a tolerance on the final condition are pre-computed and provided to the controller. This information is passed initially through the feedback differential drag algorithm and then to the feed-forward differential drag algorithm. Both algorithms generate a required control in either the positive or negative y direction in the LVLH frame which is then translated into a rotation command for each set of drag plates as depicted in Figure 2.

Upon completion of the feed-forward differential drag control sequence, the translational control of the spacecraft is transferred to the optimal low-thrust controller. The inputs to this controller are the position and velocity of the spacecraft in the LVLH frame but also a parameter is provided to select the period of re-computation of the controls. This parameter provides the designer with a trade-space between computation speed and optimality.

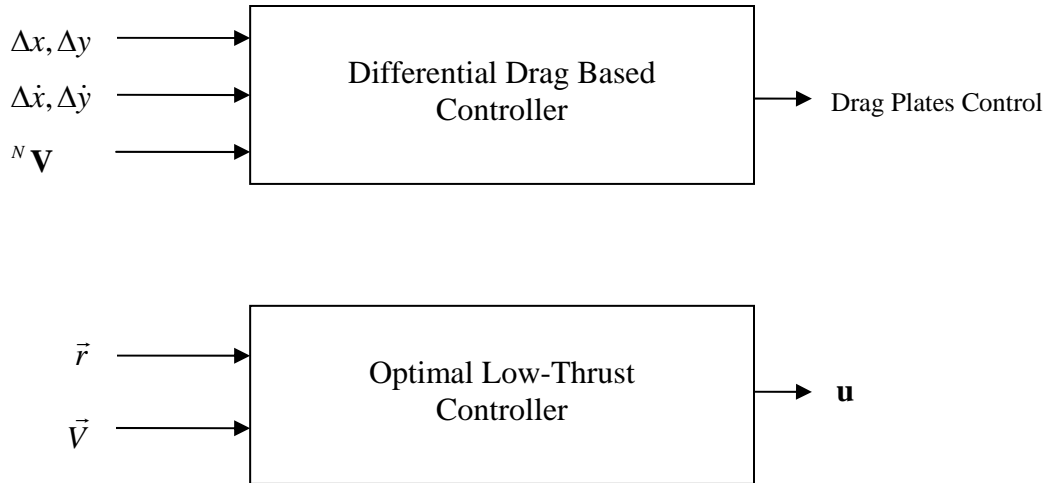


**Figure 5** Block diagram of the integrated differential drag and fuel optimal controllers

## V. Numerical Simulations

This section reports the results of two sample numerical simulations. Two chaser spacecraft and the target, described in Table 1, are maneuvering from the initial conditions reported in Table 2 and 3.

The first sample simulation employs the differential drag analytical approach described in Section II. When the analytical controller has completed its sequence, the thrusters take over, in order to reduce the residual error between the chaser spacecraft and the target spacecraft. This error is due to the assumptions made in Section II in order to develop the analytical controller. The following more realistic assumptions are considered for the simulations:

1. The atmospheric density is not constant. It is generated according to the model found in Vallado. Furthermore, a random noise of the order of magnitude of the density itself is added.
2. The dynamics is nonlinear (up to  $J_4$ ).
3. Disturbances are present (solar radiation pressure, third body effect).

The second simulation uses only thrusters on the same time frame of simulation 1, in order to compare the fuel expenditure and show the amount of saving by using differential drag.

**Table 1 Simulations Parameters**

|  |                                    |
|--|------------------------------------|
| Spacecraft Mass ( $kg$ )   | 10                                 |
| Spacecraft Main Body Face Surface Area $S$ ( $m^2$ )   | .25                                |
| Single Drag Plate Surface Area $S_p$ ( $m^2$ ) (1 of 4 for the chasers, 1 of 2 for the target) | .25                                |
| $C_D$  | 2.2                                |
| Target Altitude at Initial Time $h$ ( $km$ )   | 350                                |
| Reference Density $\rho_{350km}$ ( $kg \cdot m^{-3}$ )   | $1.3 \cdot 10^{-11}$ (Wertz, 1999) |
| Maximum Acceleration with Thrusters on $u_j$ ( $m/s^2$ ), $j = x, y, z$                        | $5 \cdot 10^{-4}$                  |
| Period of recomputation for the fuel optimal controller ( $s$ )                                | 100                                |

**Table 2 Target Spacecraft Initial Conditions**

|                                       |
|---------------------------------------|
| $a_{ISS} = 6713889.83 \text{ m}$      |
| $e_{ISS} = 0.008$                     |
| $i_{ISS} = 51.9412 \text{ deg}$       |
| $\Omega_{ISS} = 206.3577 \text{ deg}$ |
| $\omega_{ISS} = 101.0711 \text{ deg}$ |
| $\nu_{ISS} = 108.0848 \text{ deg}$    |

**Table 3 Chasers Initial Positions in LVLH**

|   |                            |
|---|----------------------------|
| Chaser 1 $[\Delta x \ \Delta y \ \Delta z]_{t=0}$ | $[1000m \ 2000m \ 10m]$    |
| Chaser 2 $[\Delta x \ \Delta y \ \Delta z]_{t=0}$ | $[-1000m \ -2000m \ -10m]$ |

## **A. Simulation Test Case 1: Differential Drag and Optimal Low Thrust Control**

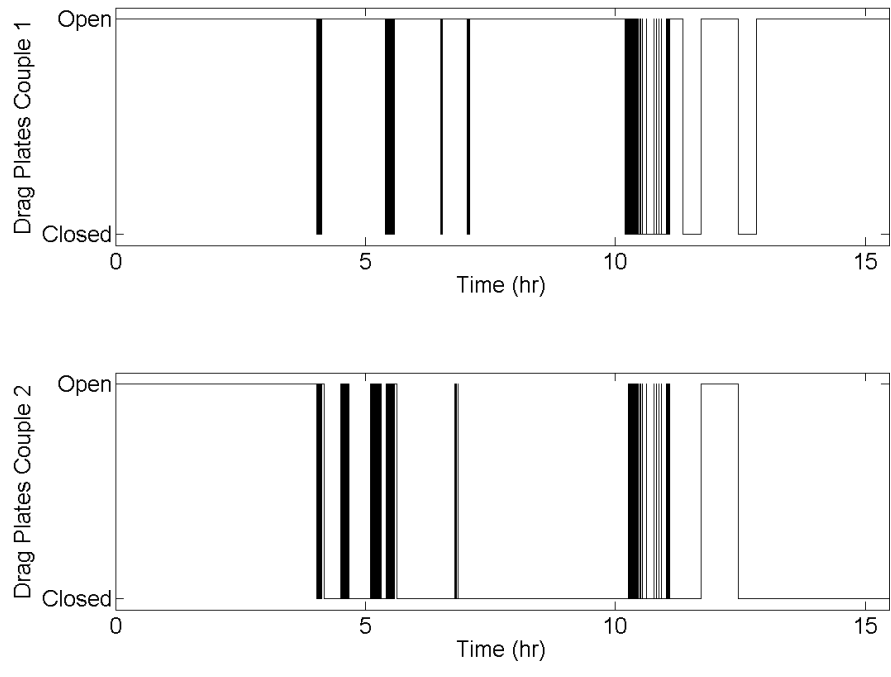
The main numerical results for Simulation Test Case 1 are reported in Table 4. The time required for completing the maneuver is 15.5 hours.

Figure 6 and Figure 7 show the drag plates control history for chaser one and two. In particular, the drag plates are supposed to be opened and closed in couples, by rotating the plates which are symmetric with respect to the spacecraft in opposite directions, so that attitude effects can be compensated (see Figure 2). It is worth to underline that the maneuver time frame is 15.5 hours, so that the rotation of the plates depicted in Figure 6 and Figure 7 is not showing chattering, the rotations occur at feasible rates.

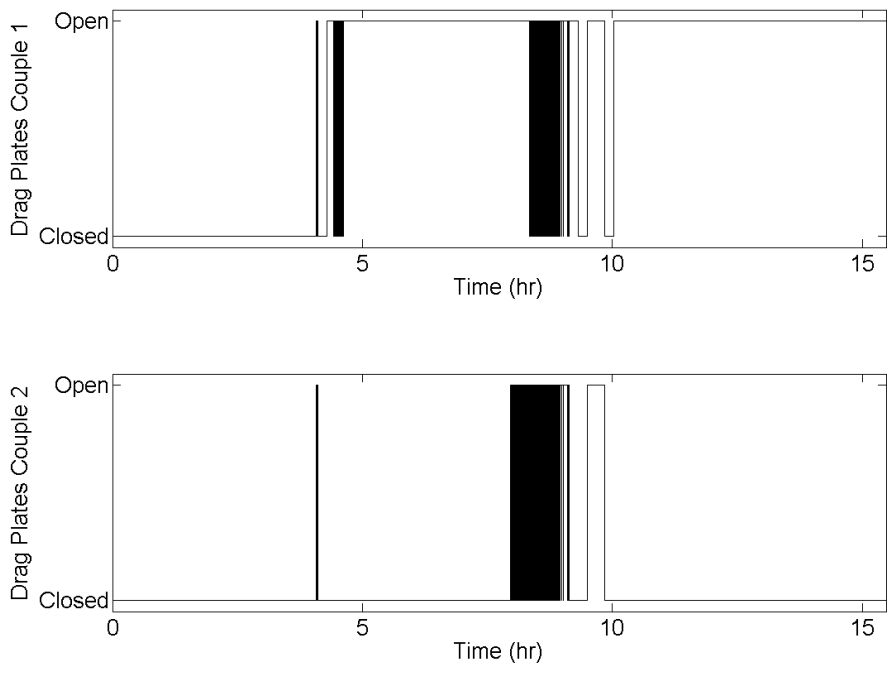
Figure 8 and Figure 9 depict the two chasers' thrust history, demonstrating active thruster control only near the end of the maneuver, after the drag controller has completed the feed-forward phase. Furthermore, Figure 8 and Figure 9 show smooth behavior for the thrust history and also that the thrust limitations are respected.

Figure 10 and Figure 11 show the rendezvous trajectories of the two chasers in different views in the LVLH reference frame. The two chasers reach the target without any collision.

Finally, Figure 12 demonstrates how the differential drag logic satisfactorily drives the chasers in the vicinity of the target before the fuel optimal controller takes over.



**Figure 6 Drag Plates Control Sequence for Chaser 1.**



**Figure 7 Drag Plates Control Sequence for Chaser 2.**

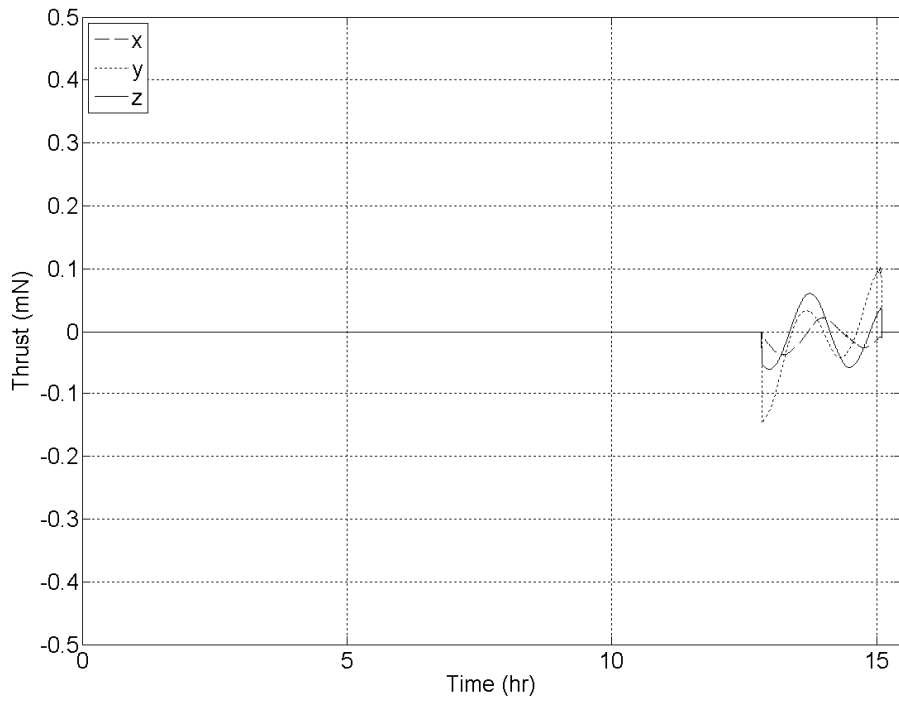


**Figure 8 Low Thrust Control Sequence for Chaser 1: Differential Drag and Thrusters.**

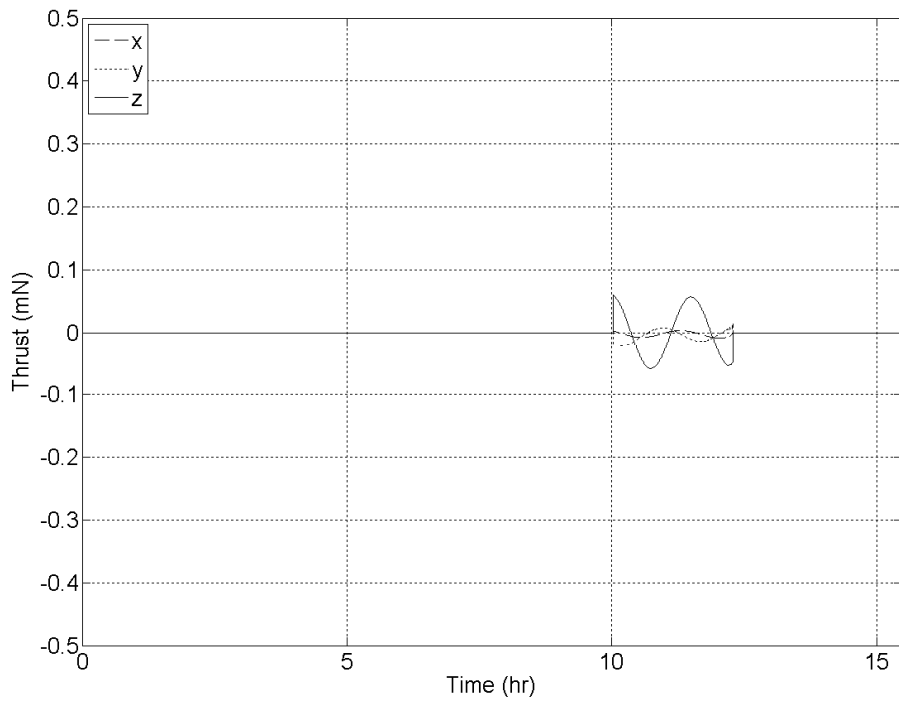


**Figure 9 Low Thrust Control Sequence for Chaser 2: Differential Drag and Thrusters.**

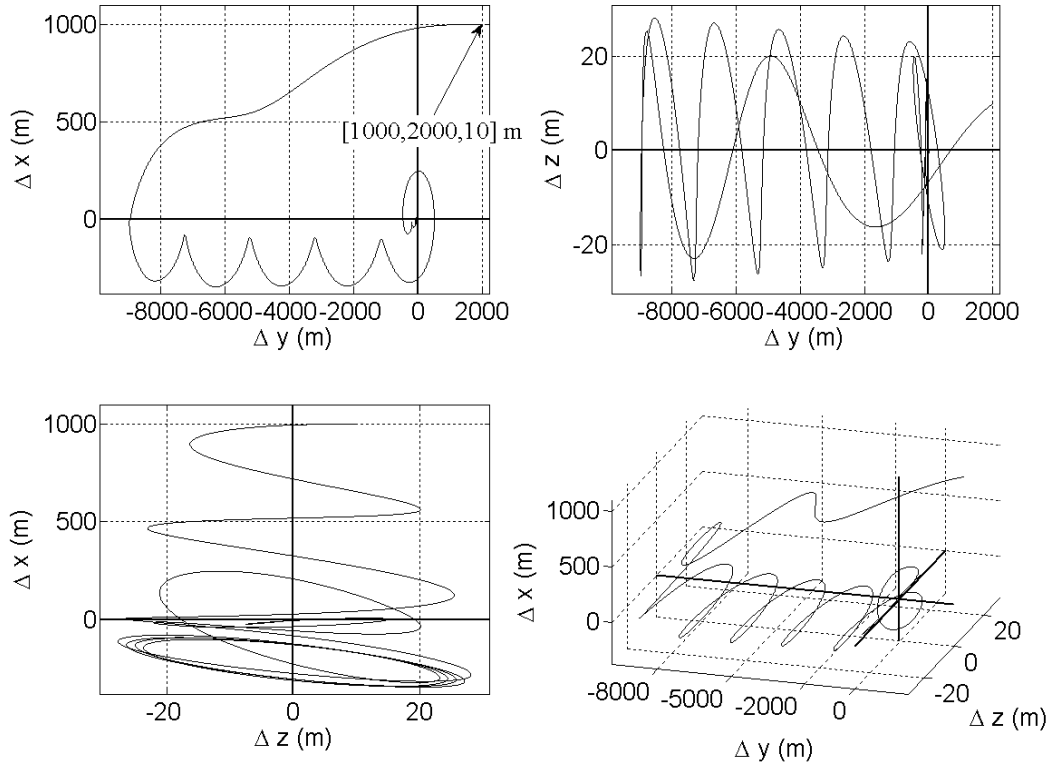


**Figure 10 Trajectory of Chaser 1: Differential Drag and Thrusters.**

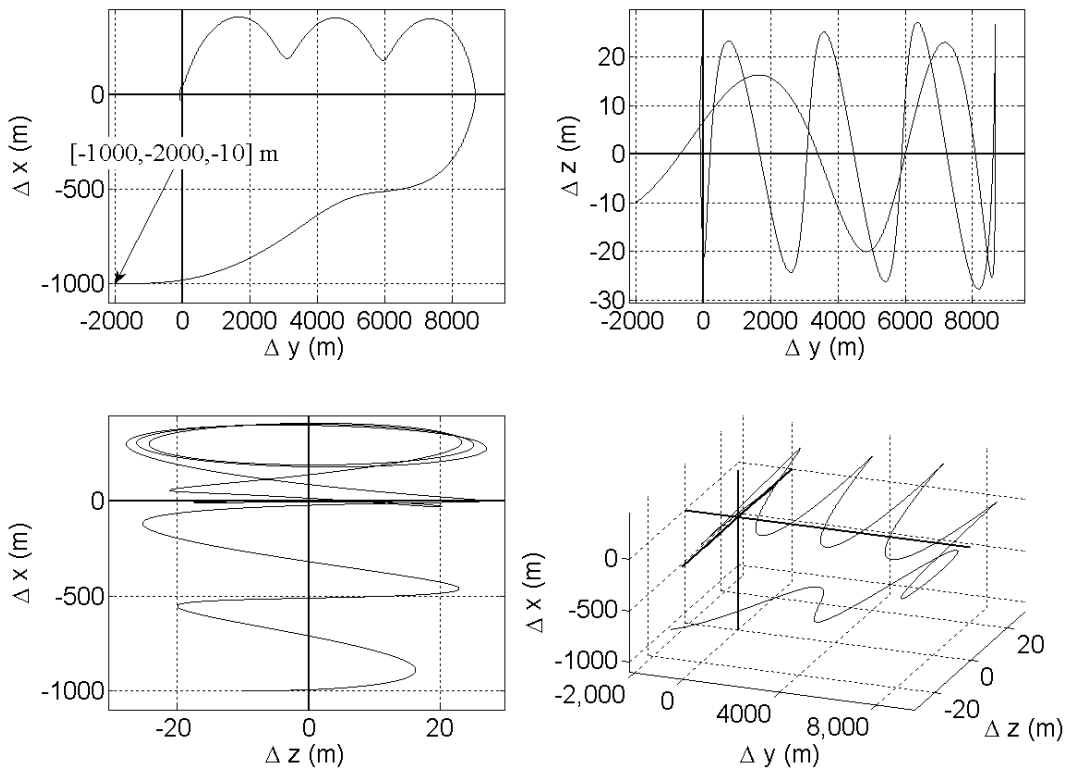


**Figure 11 Trajectory of Chaser 2: Differential Drag and Thrusters.**

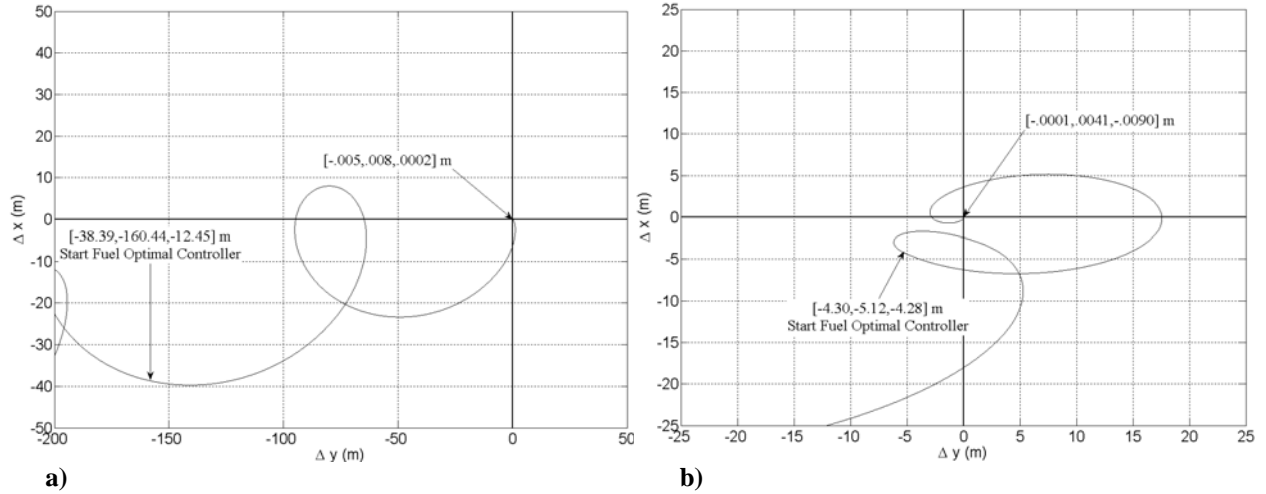


**Figure 12 Last Phases of the Trajectories of Chaser 1 (a) and Chaser 2 (b): Differential Drag and Thrusters.**

Further advantage of the proposed new drag plates' concept is that no coasting phases are required with respect to the work of Bevilacqua and Romano, 2008, optimizing the overall maneuver required time.

**Table 4 Simulation 1 Results: Fuel Consumption for the propelled phase**

| Chaser 1                         | Chaser 2                         |
|----------------------------------|----------------------------------|
| Impulse $I = 0.80317 \text{ Ns}$ | Impulse $I = 0.40405 \text{ Ns}$ |
| $\Delta V = 0.08032 \text{ m/s}$ | $\Delta V = 0.0404 \text{ m/s}$  |

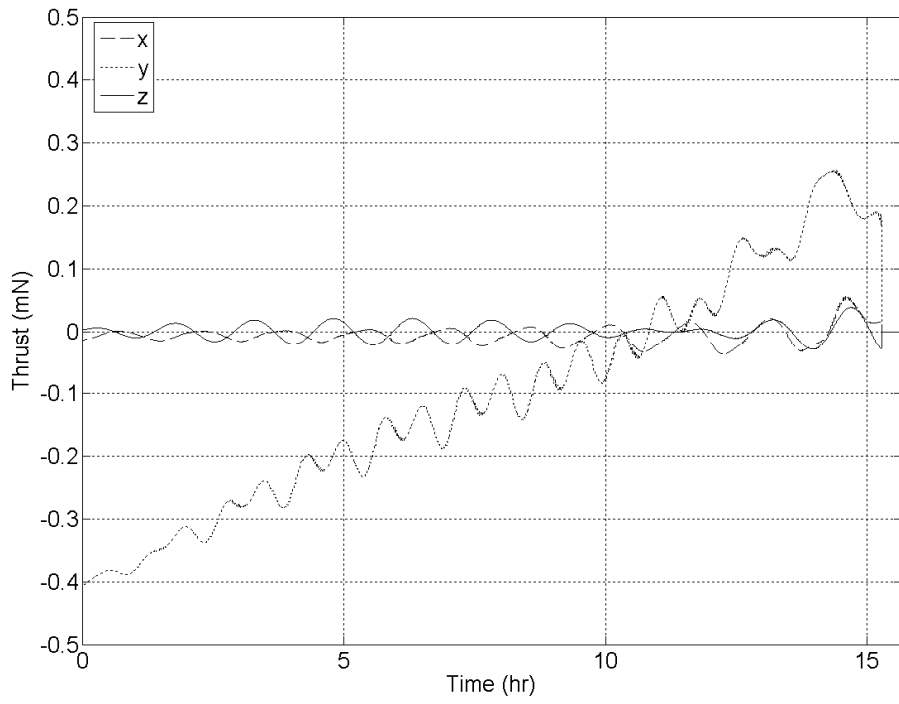
## B. Simulation Test Case 2: Optimal Low Thrust only

The main numerical results for Simulation Test Case 2 are reported in Table 5. The time imposed for completing the maneuver is the same of the simulation with aero drag and thrusters, i.e. 15.5 hours.

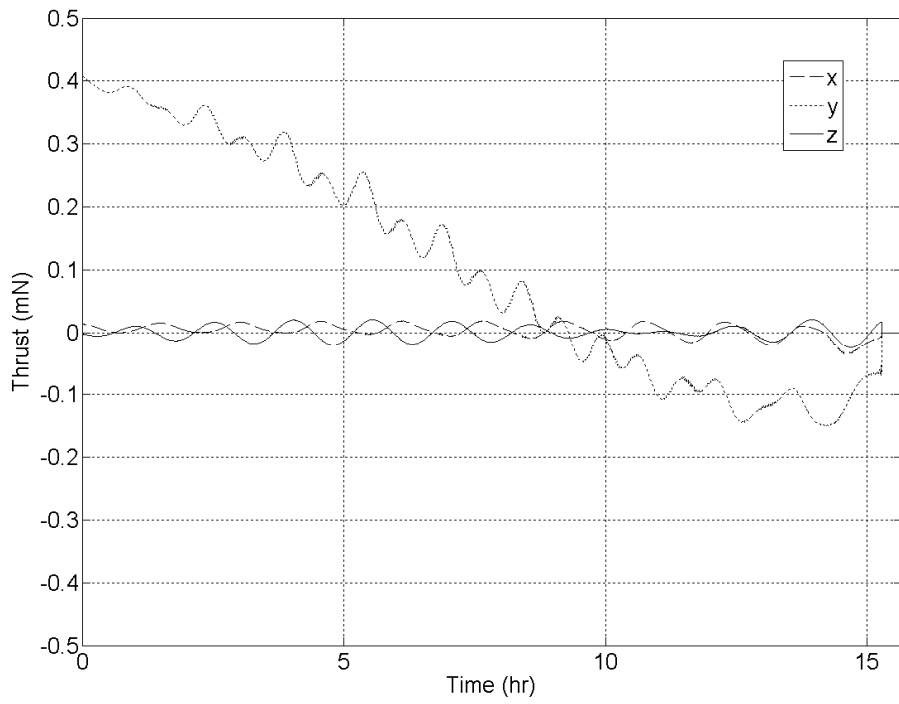
Figure 13 and Figure 14 are the chasers' thrust histories when the maneuver is performed using thrusters only. In this simulation the engines are used throughout the whole maneuver and the thrusters' capability is exploited more than in the previous simulation, still maintaining a smooth profile and respecting the constraint on the maximum allowed acceleration on each direction.

Figure 15 and Figure 16 show the rendezvous trajectories of the two chasers in different perspective in the LVLH reference frame. Both the chasers reach the target state vector.

As expected, comparison of Tables 4 and 5 yields a propellant savings for the combined differential drag and low-thrust controller against the low-thrust controller of 92%.



**Figure 13 Low Thrust Control Sequence for Chaser 1: Thrusters only.**



**Figure 14 Low Thrust Control Sequence for Chaser 2: Thrusters only.**

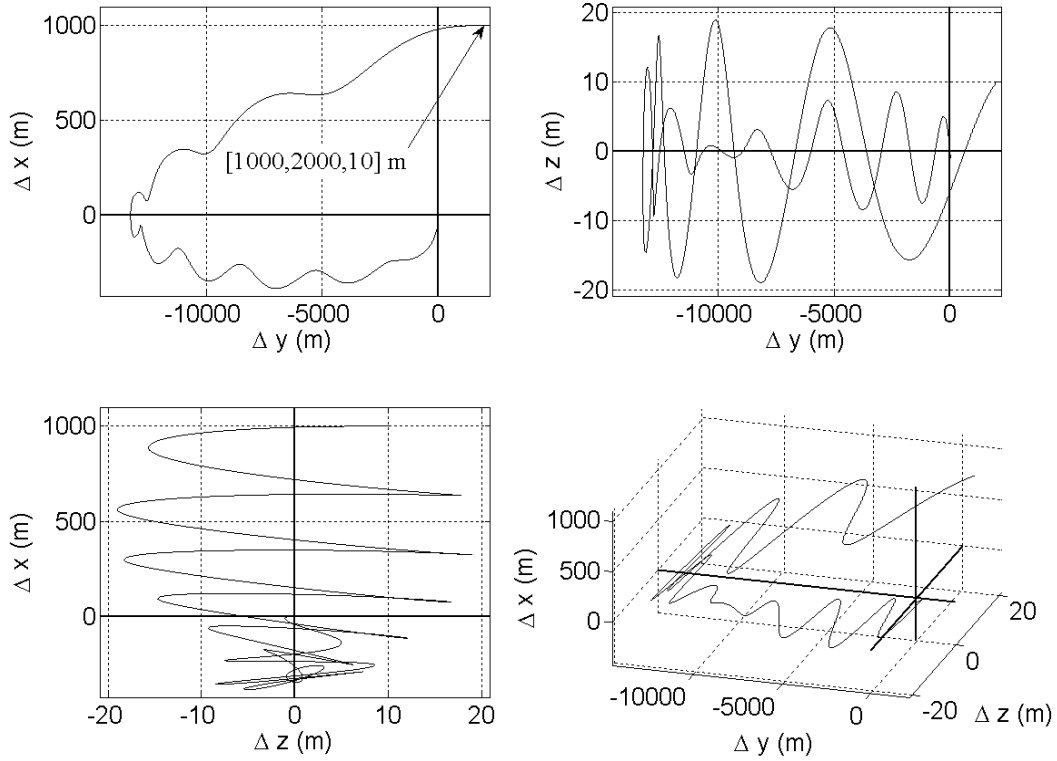


**Figure 15 Low Thrust Control Sequence for Chaser 1: Thrusters only.**

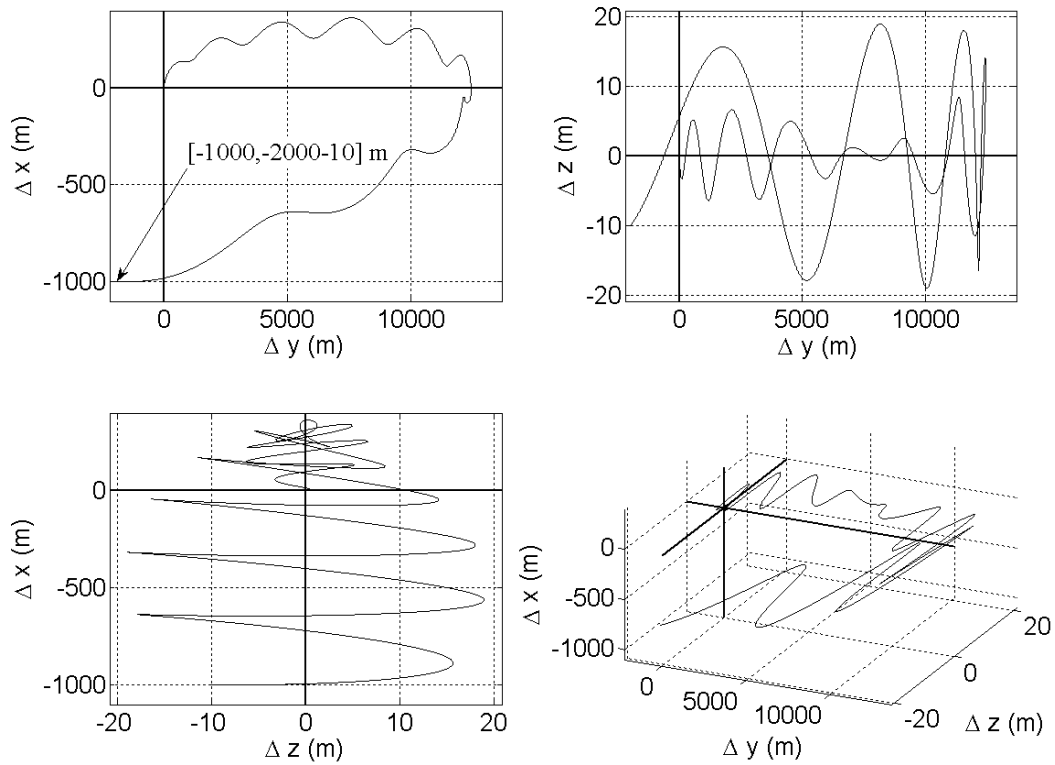


**Figure 16 Low Thrust Control Sequence for Chaser 2: Thrusters only.**

**Table 5 Simulation 2 Results: Fuel Consumption for the maneuver**

| Chaser 1                         | Chaser 2                         |
|----------------------------------|----------------------------------|
| Impulse $I = 10.9700 \text{ Ns}$ | Impulse $I = 10.4686 \text{ Ns}$ |
| $\Delta V = 1.0971 \text{ m/s}$  | $\Delta V = 1.0469 \text{ m/s}$  |

## VI. Conclusion

This work presents a hybrid technique which enables multiple-spacecraft rendezvous and assembly to a target spacecraft with low usage of propellant. The combination of differential drag from far away distances and low-thrust engines for the final approach to the target is the key factor of this research. In particular, the spacecraft are considered equipped with drag plates whose orientation can be changed with respect to the atmosphere wind direction, in order to control the amount of differential drag among them. In the final phase of the maneuver, a fuel optimal continuous low-thrust controller drives the spacecraft to the target. Both the differential and fuel optimal controllers are based on linear dynamics, but are demonstrated here to be feasible solutions for a high fidelity model of the orbital environment with its nonlinear effects, including solar, atmospheric, third body and up to  $J_4$  gravitational effects.

Starting from a previous work by the authors, important developments are here presented for the completely analytical differential drag approach. In particular, the drag plates' concept is improved with respect to previous work by the authors, so that shorter time frames are required for maneuvering the spacecraft. Furthermore, new analytical breakthroughs are reported for the closed form solution control sequence based on differential drag.

The simulations confirm the advantage of using differential drag with respect to an optimal use of thrusters in terms of propellant consumption. Furthermore, the concept of variable drag plates on each of the chaser spacecraft provides a feasible and low-risk ability to generate requisite drag differentials.

## Acknowledgments

This research was partially supported by DARPA. This research was performed while Dr. Bevilacqua was holding a National Research Council Research Associateship Award at the Spacecraft Robotics Laboratory of the US Naval Postgraduate School.

## References

- Balaji Shankar Kumar, Alfred Ng, 2008, "A Bang-Bang Control Approach to Maneuver Spacecraft in a Formation with Differential Drag", **AIAA Guidance, Navigation and Control Conference and Exhibit**, Honolulu, Hawaii, Aug. 18-21.
- Bevilacqua, R, Romano, M, 2008, "Rendezvous Maneuvers of Multiple Spacecraft using Differential Drag under J2 Perturbation," *AIAA Journal of Guidance Control and Dynamics*, Vol. 31, no. 6, pp. 1595-1607.
- Bevilacqua, R., Romano, M., 2007, "Optimal Guidance of Proximity Maneuvers for a Spacecraft with Hybrid On-Off Continuous and Impulsive Thrust," *AIAA Journal of Guidance, Control, and Dynamics*, Vol. 30, Issue 4, pp. 1175-1178.
- Campbell, M. E., 2003, "Planning Algorithm for Multiple Satellite Clusters," *Journal of Guidance, Control, And Dynamics*, Vol. 26, No. 5, pp. 770-780.
- Carter, T., and Humi, M., 2002. "Clohessy-Wiltshire Equations Modified to Include Quadratic Drag," *AIAA Journal of Guidance, Control and Dynamics*, Vol. 25, No. 6, pp. 1058-1063.
- Clohessy W. H., and Wiltshire R. S., 1960 "Terminal Guidance System for Satellite Rendezvous," *Journal of the Aerospace Sciences*, Vol. 27, No. 9, pp. 653-658.
- Guelman, M., Aleshin, M., 2001, "Optimal Bounded Low-Thrust Rendezvous with Fixed Terminal-Approach Direction," *AIAA Journal of Guidance, Control, and Dynamics*, Vol. 24, No. 2, pp. 378-385.
- Humi, M., and Carter, T., 2001, "Fuel-Optimal Rendezvous in a Central Force Field with Linear Drag," *Paper AAS 01-236*, pp. 1875-1892.
- Humi, M., and Carter, T., 2003, "Motions in a Central Force Field with a Quadratic Model," *Paper AAS 03-238*, pp. 2005-2018.
- Kumar, K. D., Bang, H. C., Tahk, M. J., 2007, "Satellite Formation Flying using along-track thrust," *Acta Astronautica*, Vol. 61, pp. 553-564.
- Leonard, C. L., 1986, "Formationkeeping of Spacecraft Via Differential Drag," *M. Sc. Thesis, Massachusetts Institute of Technology*, Cambridge, MA.
- Leonard, C. L., Hollister, W., M., and Bergmann, E. V., 1989 "Orbital Formationkeeping with Differential Drag," *AIAA Journal of Guidance, Control and Dynamics*, Vol. 12, No. 1, pp. 108-113.

Maclay, T., Tuttle, C., 2005, "Satellite Stationkeeping of the ORBCOMM Constellation Via Active Control of Atmospheric Drag: Operations, Constraints, and Performance", *Advances in Astronautical Sciences*, Vol. 120, Part I, pp. 763-773.

Palmerini, G. B., Sgubini S., Taini, G., 2005, "Spacecraft Orbit Control Using Air Drag," *Paper IAC-05-C1.6.10*.

Pontryagin, L.S., Boltjanskiy, V.G., Gamkrelidze, R.V., and Mishenko, E.F., 1969, "The Mathematical Theory of Optimal Processes", *Wiley-Interscience*, New York, NY, pp 27-35.

Schweighart, S. A., Sedwick R. J., "High-Fidelity Linearized  $J_2$  Model for Satellite Formation Flight," 2002, *AIAA Journal of Guidance, Control, and Dynamics*, Vol. 25, No. 6, pp. 1073-1080.

Starin, R. S., Yedavalli, R. K., Sparks, A. G., 2001, "Spacecraft Formation Flying Maneuvers Using Linear-Quadratic Regulation with No Radial Axis Input," *AIAA Paper 2001-4029, AIAA Guidance, Navigation, and Control Conference and Exhibit, Montreal, Canada*.

Vallado, D. A., "Fundamentals of Astrodynamics and Applications," Second Edition, *Microcosm Press*, final table before cover, no page number.

Wertz J. R., Larson W. J., "Space Mission Analysis and Design," Third Edition, *Space Technology Series* 1999, final table before cover, no page number.